CHINESE JOURNAL OF MECHANICAL ENGINEERING
Vol. 27, No. 1, 2014

DOI: 10.3901/CJME.2014.01.154, available online at www.springerlink.com; www.cjmenet.com; www.cjmenet.com.cn

Design and Experiment of ϕ-type-knots Knotters on Chinese Small Square Balers

LI Hui[1], HE Jin[1, *], WANG Qingjie[1], LI Hongwen[1], RASAILY Rabi Gautam[2, 3], CAO Qingchun[3], and ZHANG Xiangcai[1]

1 *Beijing Key Laboratory of Optimized Design for Modern Agricultural Equipment, College of Engineering, China Agricultural University, Beijing 100083, China*
2 *Agricultural Engineering Division, Nepal Agricultural Research Council, Lalitpur, Kathmandu, Nepal*
3 *Henan Hao Feng Machinery Manufacturing Co., Ltd., Henan 461103, China*

Received December 25, 2012; revised September 9, 2013; accepted September 16, 2013

Abstract: Since the knotters on the Chinese rectangular balers are imported from outside of the country, Chinese knotters with independent intellectual property rights is far away from being closed. In order to harvest a large quantity of straw in a short period on the small-scale lands of China, basic requirements on the knotters are summarized. Mathematical model of the knotter is also determined uniquely. Furthermore, the ϕ-type-knots knotter equipped on the Chinese square baler to form the ϕ type knots is designed. Knotting rate experiments of the ϕ-type-knots knotter on the test bench and in the wheat/maize straws covered fields are carried out to check the knotting performances of the knotter. The parameters of the formed knots are also tested. The experiments results show that the knotting rate of the ϕ-type-knots knotter reaches 100.0% on the test bench without straws, while reaches 99.6% in the wheat straws covered field and 100.0% in the maize straws covered field. The average maximum force in the knotting process is 194.7 N in the lab experiment. The length out of the knots formed in lab is 15.9%–20.6% lower than the knots formed in the field experiment. The breaking force of the knots formed in the field is 115.9%–167.2% higher than the knots formed in lab due to the higher preload and interactions with the compacted bales. Highly relevant relationships exist between the breaking force of the formed knots and the maximum force in the forming process of the knots in the lab experiment. The designed knotter breaks out the embarrassing situation of the domestic knotters which don't have independent intellectual property rights, and promotes the development of Chinese knotter technology, and the mathematical model is helpful for designing new type of knotters.

Keywords: small square baler, knotter, mechanical design, spatial parameters, time sequence.

1 Introduction

China produces 700 million tones of straws annually[1], which is a large amount of easily accessible renewable-energy resource. However, only 50% of these straws are used for cooking, animal feeding, and paper-making. The rest straws are burnt in the fields after grain harvest, which is not only a waste of valuable resources, but also a source of local and global pollution because of incomplete combustion[2–4]. As a potential green energy resource, it is thus necessary to bale these crop straws for easy storage or transport to some factories. The main equipment for straw recycling industry is square balers that form the straw into the square shape of the containers in vehicles. The knotter, which is used for packing the compacted straw bales, is the key component of the square baler.

The automatic baler and knotter technology began in the 19th century in the USA and Germany, where the planting areas and machines are both large[5]. The first knotter using twines were invented by APPLEBY[6]. Furthermore, the first baler using the twine knotter was fabricated by William Deering company[5]. Then the D and C type twine knotters were designed[6–7] and their constructions were further simplified[8–9]. Meanwhile, components or even the parts of the knotters were also optimized, e.g., the knotter driving pulley[10], knotter hook[11], knife lever component[12] and twine holding disk[13]. In the last decade, the standardized commercial D and C type knotters were made by WERNER[14] and VINCENT[15]. Since the knotters were easily invalid when their working environment was filled by the straws, the air blowers were imported to the large balers to blow the straws away from the knotters[16].

Nevertheless, the knotting environment in China is rugged. The knotters in China are all imported from Germany, USA, etc. The price of the imported knotter is more than 2 times of the price in abroad, and more than 20% of the total price of the domestic balers. Since the

* Corresponding author. E-mail: hejin@cau.edu.cn
This project is supported by Program for Changjiang Scholars and Innovative Research Team in University of China (Grant No. IRT13039) National Natural Science Foundation of China (Grant No. 51175499), Beijing Municipal Natural Science Foundation of China (Grant No. 6112015), and Chinese Universities Scientific Fund (Grant No. 2012YJ091)

imported knotter is equipped on small square balers without blower and work at high intensity to bale the large quantity of straws in a short period due to the multiple cropping systems, the imported knotter is not appropriate. For example, in Hwang-Huai-Hai plain of China, each province produces about 16 t ha^{-1} yr^{-1} corn straws and 7 t ha^{-1} yr^{-1} wheat straws. The straw should be baled only in 3–5 fallow days in a year[17–18]. The technology of developing domestic knotters which well suited to Chinese balers and planting systems is at the beginning in China. Structures of commercial C and D type knotters were reconstructed by YANG[19] and SU[20] by using reverse engineering technology initially. The movement of D type knotter was analyzed and simulated by LI, et al [21], YIN, et al[22], and HUANG, et al[23]. LI, et al[21, 24–25], designed key parts of knotter and tested their knotting rates. However, the research of domestic knotters is far away from being closed. In this paper, the ϕ-type-knots knotter are designed according to the working principle of the D type knotter[14], the parameters of the small square balers manufactured in China, and the features of the baled straws.

2 Knotting Conditions and Requirements

In China, a successful knotter should at least satisfy the following requirements: (1) It equips well with the small square balers; (2) It cooperates stably with the Chinese twine to form the knot successfully without breaking it; (3) It is strong enough to overcome the tension caused by the compacted bales and to accomplish the high intensity baling work; (4) It can form knots with high knotting rate and tight the compacted bales effectively[26].

Different types of small square balers almost have the same cross-sectional area of 360 mm×460 mm, and the length of the compacted bale can be adjusted in the range of 300– 1 300 mm in China[27]. The qualified twine used in the baler is polypropylene rope with different diameters of 2.5 mm (maximum tension of 518.4 N and elongation of 79.9%) and 3.5 mm (maximum tension of 845.7 N and elongation of 62.5%). Therefore, the interaction force between the knotter and the twine should be less than the maximum tension of the twine.

In Hwang-Huai-Hai plain of China, the small square balers are usually used to harvest the wheat and maize straws. During the knotting process[28–29], the force in the twine is shown in Fig. 1, which is the same as the force applied by the knotter to grip the twine. The wheat and maize compressed straws are distributed homogeneously and isotropically, respectively. Therefore, the compressive stress $\sigma_1=\sigma_2=\sigma_3=\sigma_4=\sigma$, and is given by

$$F = F_1 = F_2 = F_3 = F_4 = \frac{\sigma s l_1}{2} = \frac{\sigma s l_2 + \int_0^{l_2} g_l \mathrm{d}l}{2}, \quad (1)$$

where F—Force in the twine,

d—Diameter of the used twine,

s—Actual contact length between the twine and the bale, and $s \le d$,

g_l—Vertical stress caused by the gravity,

σ—Cmpressive stress in the bale,

l_1—Length of the bale,

l_2—Height of the bale.

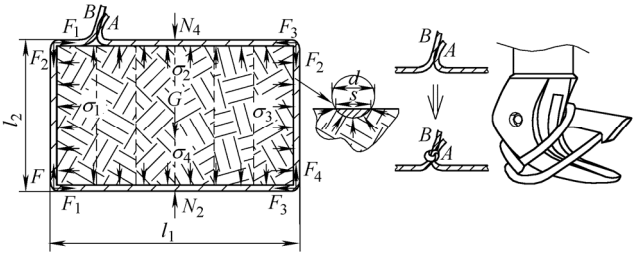

Fig. 1. Stress analysis of the bale and twine in the knotting process

Maximum and equilibrium compressive stresses are about 0.037 MPa and 0.021 MPa for the compressed wheat bales, and about 0.047 MPa and 0.021 MPa for the compressed maize bales with the cross-sectional area of 360 mm×460 mm[30–32]. During the knotting process, the knotter was working with the maximum compressive stress of the bale, while the formed knot was bearing the equilibrium stress of the bale after the knotting process.

From Eq. (1), if we choose the safety factor to be 1.5[33], then the knotter should afford the force of 307.1–586.6 N when the twine diameter is 2.5–3.5 mm, to conquer the maximum compressive stress. The formed knot should afford the force of 176.5–265.2 N when the twine diameter is 2.5–3.5 mm, to overcome the equilibrium compressive stress.

In this paper, we designed the ϕ-type-knots knotter from the time sequence (to insure the knotting rate), the spatial distribution (to keep the knotting rate and make the knotter equipped well with the balers) and the mechanical structures (to satisfy the high intensity baling work).

3 System Design

As shown in Fig. 2, there are four major components in the ϕ-type-knots knotter to form the ϕ type knots, i.e., the cam mechanism, the knotter hook gear mechanism, the twine holding gear mechanism, and the worm-helical gear mechanism. The time sequences of the four components are set by the knotter driving pulley while their relative spatial structures are fixed when mounted on the knotter frame.

3.1 Time sequence design

The knotter ties the ϕ type knots through 8 movements (shown in Fig. 3), i.e., movement I-matching the twine (realized by the needle mechanism of the square baler), movement II-gripping the end of the twine (realized by twine holding subcomponent which got the power from the

twine holding gear mechanism and worm-helical gear mechanism), movement III-rotating the twine in a circle, movement IV-knot hook opening to let the twine cross the circle and then forming the ϕ type circle, movement V-knot hook closing to hold the crossed part of the twine, movement VI-tightening the twine, movement VII-cutting the end of the ϕ type circle, movement VIII-stripping off the outside circle of the ϕ type twine and then the encased ϕ type knot being finally formed (cam mechanism). Movements III-VI are realized by the knotter hook gear mechanism, and the movements VII-VIII are realized by the cam mechanism.

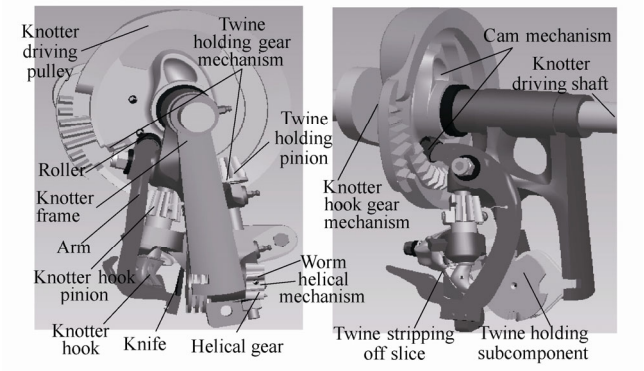

Fig. 2. Model of the ϕ-type-knots knotter

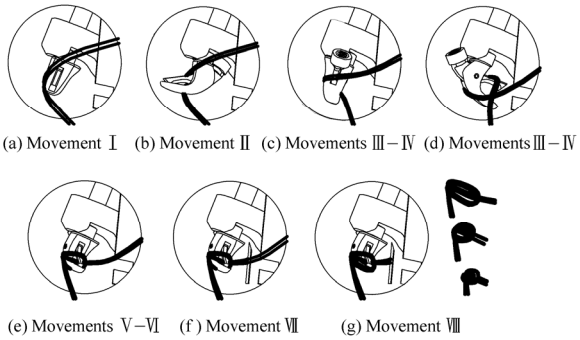

Fig. 3. 8 movements of the ϕ-type-knots knotter

The sequence of the knotting process is decided by the knotter driving pulley (Fig. 4). The sequence is established through arranging their active part on the knotter driving pulley in its 360° at the *xoy* coordinate system. 8 movements mainly act as the intermittent gear mechanisms and cam mechanisms, and are given as

$$\theta_{\mathrm{I}}+\theta_{\mathrm{II}}+\theta_{\mathrm{III\text{-}VI}}+\theta_{\mathrm{VII\text{-}VIII}}=360°, \tag{2}$$

where θ_{I}—Needed active angle of movement I at the knotter rotated one circle, (°),

θ_{II}—Needed active angle of movement II at the knotter rotated one circle, (°),

$\theta_{\mathrm{III\text{-}VI}}$—Needed active angle of movements III-VI at the knotter rotated one circle, (°),

$\theta_{\mathrm{VII\text{-}VIII}}$—Needed active angle of movements VII-VIII at the knotter rotated one circle, (°).

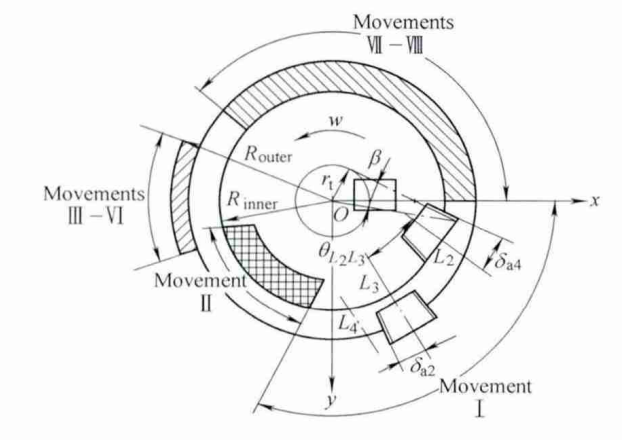

Fig. 4. Knotting processes' sequence of ϕ-type-knots knotter

w—Angular velocity of knotter driving pulley,
L_2—Transmission shaft in movement II,
L_3—Rotating shaft of movement III-VI,
L_4—Rotating shaft of movement VII-VIII,
r_t—Tangential radius of inner gear on knotter driving pulley, mm,
β—Helix angle of inner gear on knotter driving pulley, (°),
$\theta_{L_2L_3}$—Crossing angle of twine holding gear mechanism and knotter hook gear mechanism, (°),
R_{outer}—Outer cone distance of knotter hook gear mechanism, mm
R_{inner}—Inner cone distance of twine holding gear mechanism, mm
δ_{a2}—Apex angle of knotter hook active gear, (°),
δ_{a4}—Apex angle of twine holding active gear, (°).

As shown in Fig. 4, the needle is active and the twine holding gear mechanism and knotter hook gear mechanism are stopped at movement I. Therefore, the θ_{I} should be big enough for the remain of the knotter hook and the twine holding gear mechanisms, and is given by

$$\theta_{\mathrm{I}}\geq \theta_{L_2L_3}+\delta_{\mathrm{a4}}+(\delta_{\mathrm{a2}}+\beta). \tag{3}$$

According to the characteristics of gear parameters [34–35], Eq. (3) is changed into

$$\theta_{\mathrm{II}} \geq \theta_{L_2L_3}+\left\{\arctan\frac{z_4}{z_3}+\arctan\left[\frac{2\sin(\arctan(z_4/z_3))}{z_4}\right]\right\}+\left\{\arctan\frac{z_2}{z_1}+\arctan\left[\frac{2\sin(\arctan(z_2/z_1))}{z_2}\right]\right\}+\beta. \tag{4}$$

Then, the needed active angle of movemet II is given as

$$\theta_{\mathrm{II}}=360°\times(z_4/z_3). \tag{5}$$

Meanwhile, the needed active angle of movemets III-VI is given by

$$\theta_{\mathrm{III\text{-}VI}}=360°\times(z_2/z_1). \tag{6}$$

Since the knotter hook gear mechanism is moved after the twine holding gear mechanism, the twine holding gear mechanism should moved at last 2 teeth before the next

active mechanism. So the crossing angle is given as

$$\theta_{L2L3} \geq 360° \times (2/z_3). \tag{7}$$

Therefore, the time sequence of a knotting process is distributed as movement I [0, θ_I], movement II [θ_I, θ_{II}], movements III-VI [$\theta_I+\theta_{II}$, $\theta_I+\theta_{II}+\theta_{III\text{-}VI}$], and movements VII-VIII [$\theta_I+\theta_{II}+\theta_{III\text{-}VI}$, 360°]. They are all highly relevant with the mechanical parameters.

3.2 Mechanical structures

The bale length l_1 formed by the rectangular baler is 300–1 300 mm. According to the standard of knotters of rectangular balers[26], the knotter should bale at last 60 bales in 10 min. The plunger of the rectangular baler bales ≥50 mm[26–27] length of straws each time. The knotter and the needle mechanism rotates simultaneously, and there is no interference among the knotter, needle mechanism and the plunger, therefore,

$$n_k \geq n_p, \tag{8}$$

$$\frac{1}{n_p} \times \frac{l_1}{50} \leq \frac{10}{60}, \tag{9}$$

where n_k is rotated speed of the knotter (r/min), n_p is rotated speed of the plunger (r/min). Since the highest velocity of the plunger in the rectangular balers could reach 100 min^{-1}, the rotated speed of the knotter n_k=40–100 r/min.

3.2.1 Parameters of twine holding gear mechanism

The twine holding gear mechanism and the worm-helical gear mechanism for twine holding are designed to hold the twine reliably in a changed direction. The twine holding subcomponent of the ϕ-type-knots knotter works at 4 working positions, i.e. matching position-twine holding position-twine clearing off position-waiting position, to form the knots continuously (Fig. 5). As shown in Fig. 6, the needle mechanism consists of crank-link mechanism and its pivot angle θ_{TH} is 90° in Chinese rectangular balers.The contact angle θ_N between the twine holding subcomponent and the needle mechanism is 5°. The twine holding subcomponent has to hold the twines immediatelywhen the needle mechanism matches the twine. Therefore,

$$\frac{\theta_N}{\theta_{TH}} \times \frac{1}{n_k} = \frac{1}{4n_4}, \tag{10}$$

where n_4—Rotated speed of the twine holding subcomponent.

Then the transmission ratio n_k/n_4 of the twine holding gear mechanism is 1/4.5. According to the 4 positions, the transmission ratio of the worm-helical gear mechanism is 4.

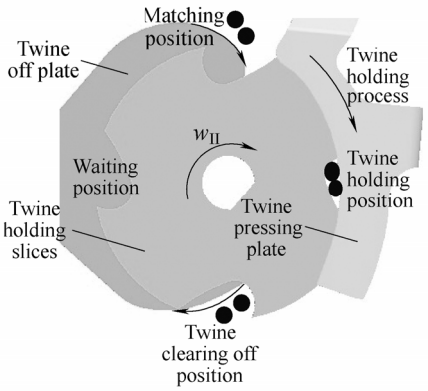

Fig. 5. Structures of twine holding subcomponent

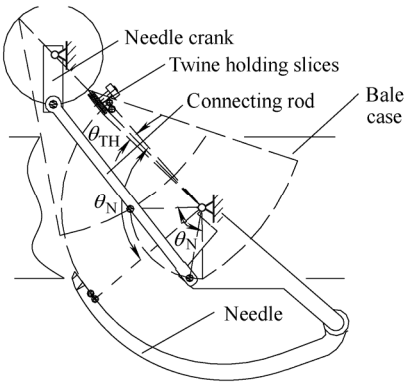

Fig. 6. Relationship between movements I and II

As shown in Fig. 7, the twine holding gear mechanism is made up of the twine nipped pinion, the worm shaft and the inner gear segment of knotter driving pulley. And the worm-helical gear mechanism consists of the knotter worm, the helical gear and the twine holding mechanism.

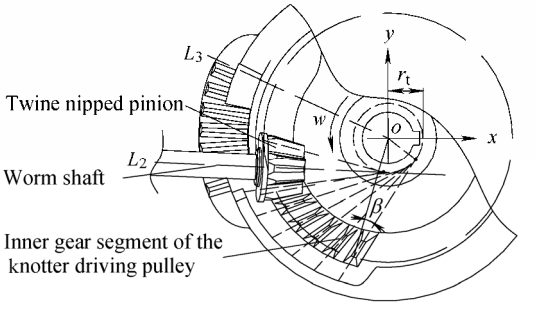

Fig. 7. Structures of the twine holding gear mechanism

The twine holding intermittent gears are designed as offset involute bevel[34–35]. According to the transmission ratio, the imaginary teeth number of the inner gear segment (z_3) and the knotter hook pinion (z_4) are designed to be 36 and 8, respectively. As the intermittent gear, the number of the actual manufactured teeth is 7. The tangential radius r_t and the helix angle β of the inner gear are 16.0 mm and 12.0°, respectively. The shaft angle δ between the twine holding pinion and the driving pulley is chosen as 98° and the manufacturing angle φ in the pinion is 90°. The range of

the modulus m_2[36] in this component is expressed as

$$m_2 \geq \sqrt[3]{\frac{4KT_2\cos^3\beta}{\phi_{R4}(1-0.5\phi_{R4})^2 z_4^2\sqrt{1+u_4^2}}\frac{Y_F}{[\sigma_F]}} \text{ mm}, \quad (11)$$

where u_4 is gear ratio, 36/8, K=1.67, Φ_{R4}=0.3, z_4=8, Y_F=4.075, $[\sigma_F]$=395 MPa, n_4=450 r/min, β=12.0°. According to the stress of the twine, T_2=54.1 N • m. Then the model m_2 should be more than 3.86 mm. Therefore, the module here is determined as 4 mm in the same principle as mentioned above[36–37].

In the worm-helical gear mechanism, the teeth number of the worm and helical gear are set to be 2 and 8, respectively. The tooth profile for worm and helical gear are designed as archimedes spiral and involutes, respectively. Helix angle of the worm β_2 is decided to be 7°. The shaft angle between the worm and helical gear is 80°. In this mechanism, the normal gear module of the helical gear is also chosen as 4 mm according to the GB/T standard 1357-2008[36–37]. The distance $d_{L_2L_5}$ between the axis L_2 and L_5 is 29.0 mm.

3.2.2 Parameters of knotter hook gear mechanism

The knotter hook gear mechanism is composed of the knotter hook pinion, the knotter hook, and the outer gear segment of the knotter driving pulley. According to Eq. (7), the angle $\theta_{L_2L_3}$ between the axis L_2 and L_3 is more than 20°. In order to take full use of the time sequence of the knotter driving pulley, the action time of the movement III-VI is superimposed with the action time of the movement II. To hold the twine reliably, the twine holding gear mechanism turns 2-3 teeth before the knotter hook gear mechanism. Therefore,

$$\frac{\frac{z_4-3}{z_3}\times 360°}{2\pi n_k} < \frac{\frac{z_2}{z_1}\times 360°}{2\pi n_k} < \frac{\frac{z_4-2}{z_3}\times 360°}{2\pi n_k}, \quad (12)$$

where z_1 is imaginary teeth of the outer gear segment, z_2 is imaginary teeth of knotter hook pinion.

Then the imaginary teeth z_1 and z_2 are designed as 57 and 8, respectively, and $\theta_{L_2L_3}$ =20°–22°. The number of the actual manufactured teeth is also 7 in each of them and the positions of the other gear teeth were manufactured into plane as the locking position (Fig. 8). The shaft angle δ' between the knotter hook pinion and the driving pulley is set to be 98° and the manufacturing angle φ_1 in the pinion is 90°[37]. The locking plane on the knotter driving pulley should be sloped, and the slope angle α_1 is 8°. The matched intermittent gears for movements III-VI are designed as involute bevel gears. According to the principles of designing external involute spur gears[34], the modulus m_1 in this component is formulated as

$$m_1 \geq \sqrt[3]{\frac{4KT_1}{\phi_{R2}(1-0.5\phi_{R2})^2 z_2^2\sqrt{1+u_2^2}}\frac{Y_F}{[\sigma_F]}} \text{ mm}, \quad (13)$$

where T_1=Fd_1=59.9 N • m, and F is the stresses in the twine; K=1.67 is the load coefficient of the knotter; Φ_{R2}=0.3 is the tooth breadth-diameter ratio in this component; z_2 = 8; the gear ratio of the knotter hook gear mechanism u_2=57/8; Y_F=4.075 is the gear shape coefficient; $[\sigma_F]$=395 MPa; n_1=711.5 r/min is the rotate speed in knotter hook component. Thus, the modulus m_1 is more than 3.5 mm. According to the Chinese national standard GB 12368-90[36–37], the module of this mechanism was finally designed as 3.75 mm.

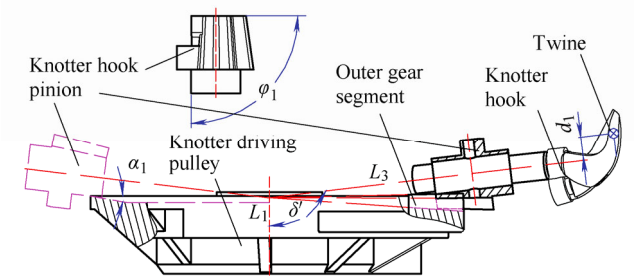

Fig. 8. Structures of the knotter hook gear mechanism

3.2.3 Parameters of cam mechanism

The cam mechanism is devised as an orthogonal oscillating disk cam mechanism. The arm is used to cut the twine and strip off the formed knot. Based on the decided parameters, $\theta_I \geq 48.2°$, $\theta_{II} \geq 70.0°$, $\theta_{III\text{-}VI} \geq 44.2°$. Then the working angle $\theta_{VII\text{-}VIII}$ of movements VII-VIII $\leq 197.6°$. As limited by the spatial space, the farthest point of the cam should be less than $d_{f3}/2$=71.5 mm. Then the farthest point of the cam is designed as 67.0 mm. And the pivot angle φ of the arm, is 26°. Meanwhile, the radius of the base circle is designed as 38 mm. The distance change trend of the cam is described in Fig. 9(a). The instability and acceleration shock pulses would reduce the working life of the cam mechanism. However, proper acceleration is needed for the motions of the arm to cut the twine and strip off the knot powerfully, so the kinetic trail with soft impulse is used here. The arm moves to the farthest position when the driving pulley rotates, and the motions are designed to finish before the lowest position.

As shown in Fig. 9(b), the acceleration reaches the highest at both sides of the farthest point of the cam, considering the arm needs higher force to finish movements VII-VIII before the point and higher force to return to the initial position after the point. The cam trajectory curve consists of five tangential circular arcs (Fig. 10(a)), and is used to maintain the surface smooth and certain accelerations.

In Fig. 10(b), the radius r of the roller is 10 mm, the theoretical base circle radius r_b of the cam is 38 mm, (O_{ix}, O_{iy}) (i=1, 2, 3, 4) are the centers of the arcs with the radius

of R_1(86.4 mm), R_2(35.4 mm), R_3(7.4 mm), R_4 (50.1 mm). The cam profile curve in the vertical plane, which is perpendicular to the tooth plate plane, is expressed as

$$h = C_4D_4 - \sqrt{C_4D_4{}^2 - (D_{L_1L_4} - OD_4)^2}\ , \qquad (14)$$

where h is instantaneous distance between the roller centre B and H, H is the lowest position of the roller centre in the vertical plane. Assuming there is no friction between the roller and cam segment, the pressure angle α is obtained from

$$\tan\alpha = \frac{D_{L_1L_4} - r_b}{C_4D_4 - h}\ . \qquad (15)$$

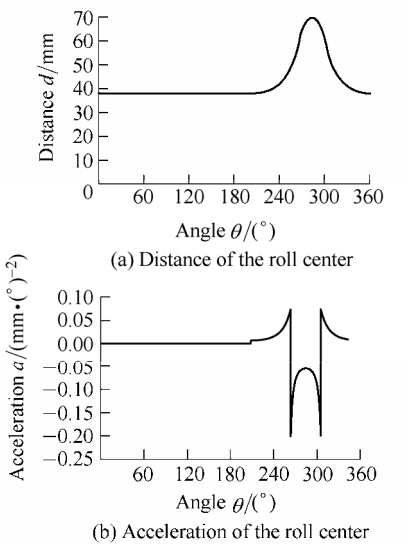

Fig. 9. Kinetic characteristics of the cam mechanism

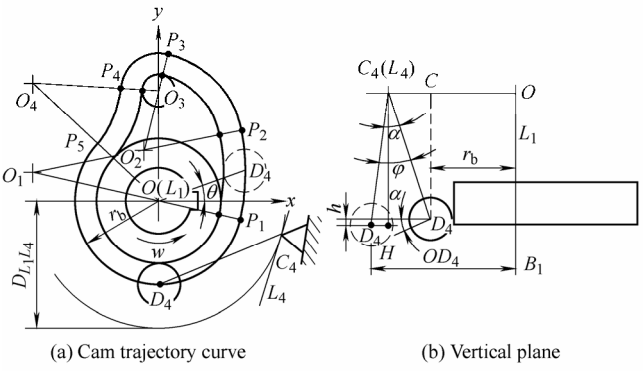

Fig. 10. Structure of the cam mechanism

The maximum press angle α_m existes at the lowest point and the value is 19.1° which less than the allowable pressure angle $[\alpha]$[33].

To cut the twine effectively and effortlessly, a cutting experiment has been done by using the RGM-4005 Material Testing Machine (Fig. 11). The experiment velocity is 200 mm/min. Since the knot stability is irrelevant with the cutting position[38], the installation angle ψ_{TC} of the cutter and the cutting angle θ_{TC} of the cutter are figured out. As shown in Fig. 12, when the cutter cuts the twine with the cutting angle of 45° and installation angle of 0°, the needed cutting force and the needed length of the cutter are optimal.

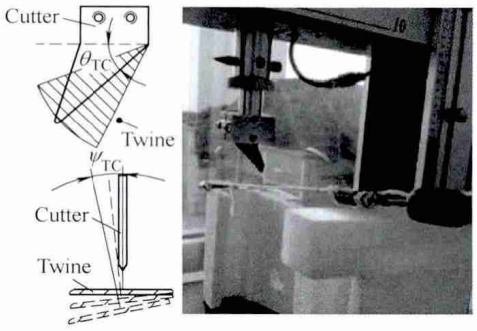

Fig. 11. Cutting experiment of the cutter

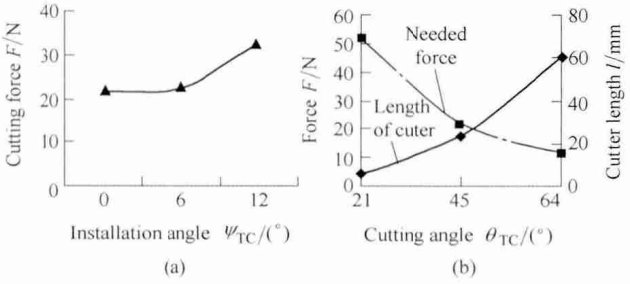

Fig. 12. Cutting results of the cutter

Depends on the above parameters, the time sequence is figured out, i.e., movement I [0°, 102°], movement II [102°, 172°], movements III-VI [160°, 207°], movements VII-VIII [220°, 360°].

3.3 Spatial distribution design

3.3.1 Model constraints

All the decided key parts are installed on the knotter frame. As shown in Fig. 13, the twine holding is crucial for the subsequent movements in the knotting process. To ensure the reliable twine holding, the spatial track of S_{II} is intersected with the twine matching tracks L_{61} and ϕ type knot. Therefore,

$$\begin{cases} |\boldsymbol{C}_{L_6L_{51}}\boldsymbol{C}_5| = |\boldsymbol{AC}_5|, \\ \cos\dfrac{\pi}{2} = \dfrac{|\boldsymbol{C}_{L_6L_{51}}\boldsymbol{C}_5 \square \boldsymbol{AC}_5}{|\boldsymbol{C}_{L_6L_{51}}\boldsymbol{C}_5 \square \boldsymbol{AC}_5|}, , \\ \boldsymbol{AC}_5 \bullet \boldsymbol{L}_5 = 0, \end{cases} \qquad (16)$$

where $\boldsymbol{A} \in \boldsymbol{L}_{CA}$, $\boldsymbol{C}_5 \in \boldsymbol{L}_5$, $\boldsymbol{C}_{L_6L_{51}} \in \boldsymbol{L}_{51}$, $\boldsymbol{C}_{L_6L_{51}} \in \boldsymbol{L}_6$.

In the movements II to VI, the well regulated move and cease of the relative components are realized by the excellent cooperation between the executive gears and the knotter driving pulley. The rotating shafts L_2 and L_3 of the executive gears are required to be parallel with the locking plane of the knotter driving pulley according to the

manufacturing technology of the intermittent bevel gear[33]. As decided above, the relationship of the angle between the vector quantity of axes L_2 and L_3 is

$$\arccos < \boldsymbol{L}_1, \boldsymbol{L}_{11} >= \arccos < \boldsymbol{L}_1, \boldsymbol{L}_2 >= \arccos < \boldsymbol{L}_1, \boldsymbol{L}_3 >,$$

$$< \boldsymbol{L}_2, \boldsymbol{L}_3 >= \arccos\left(\frac{\boldsymbol{L}_2 \bullet \boldsymbol{L}_3}{|\boldsymbol{L}_2| \bullet |\boldsymbol{L}_3|}\right) = 20^{\circ} - 22^{\circ}. \quad (17)$$

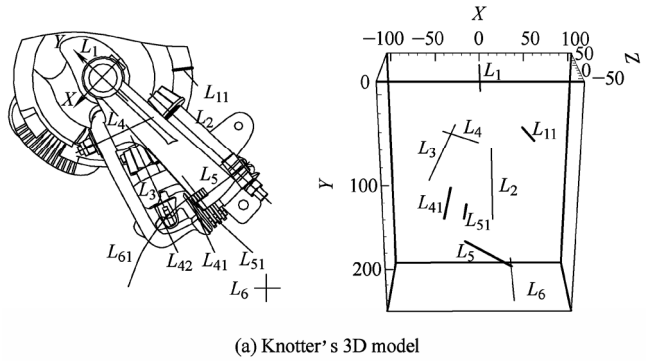

(a) Knotter's 3D model

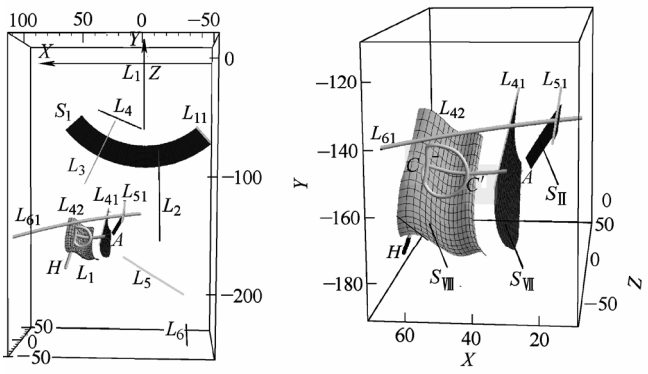

(b) Mathematical model of the knotter's key movements

Fig. 13. Spatial structure and key movement's tracks of the ϕ-type-knots knotter

L_1—Knotter driving shaft,
L_5—shaft of the twine gripper in Movement II,
L_6—Rotating shaft of the Movement I,
L_{61}—Tracks of the Movement I,
L_{11}—Generatrix of locking plane,
L_{41}—Twine cutting line,
L_{42}—Twine stripping off line,
L_{51}—Line of twine holding groove,
S_{I}—Locking plane on the driving pulley,
S_{II}—Tracks for twine gripping,
S_{VII}—Tracks for twine cutting,
S_{VIII}—Tracks for twine stripping off,
A,H—Two ends of the twines,
CC'—Semi-circle of ϕ type knot for Movement VIII.

Meanwhile, the twine holding mechanism has the relationship of

$$< \boldsymbol{L}_2, \boldsymbol{L}_5 >= \arccos\left(\frac{\boldsymbol{L}_2 \bullet \boldsymbol{L}_5}{|\boldsymbol{L}_2| \bullet |\boldsymbol{L}_5|}\right) = \frac{\pi}{2} - \beta, \quad (18)$$

$$d_{L_2L_5} = \left|\boldsymbol{D}_{L_2} - \boldsymbol{D}_{L_5}\right| = 29 \ \text{mm}, \quad (19)$$

where

$$\begin{pmatrix}\boldsymbol{D}_{L_2}\\ \boldsymbol{D}_{L_5}\end{pmatrix} = \begin{pmatrix}\boldsymbol{A}_2\\ \boldsymbol{A}_5\end{pmatrix} + k_{\mathrm{DL}}\begin{pmatrix}\boldsymbol{B}_2 - \boldsymbol{A}_2\\ \boldsymbol{B}_5 - \boldsymbol{A}_5\end{pmatrix},$$

$$k_{DL} \in [0,1], \ \begin{cases}\boldsymbol{D}_{L_2}\boldsymbol{D}_{L_5} \bullet \boldsymbol{L}_2 = 0,\\ \boldsymbol{D}_{L_2}\boldsymbol{D}_{L_5} \bullet \boldsymbol{L}_5 = 0,\end{cases}$$

and β is angle of the helical gear, 10°.

The twine cutting and stripping off are achieved by the cam (integrated with the knotter driving pulley and rotated around with L_1) driving oscillating bar (rotated along with L_4) mechanism. The relationship between L_1 and L_4 is decided by

$$\boldsymbol{L}_1 \square \boldsymbol{L}_4 = 0, \quad (20)$$

where $\boldsymbol{L}_1$, $\boldsymbol{L}_4$ are the vector quantities of the axis L_1 and L_4, respectively. Since the movements II and VII are working in the same space, the cutting surface S_{VII} shouldn't interfere with the twine gripping surface S_{II}. Therefore,

$$\boldsymbol{L}_4 // \boldsymbol{L}_5. \quad (21)$$

3.3.2 *Model building*

As shown in Fig. 13, the coordinate system XYZ is built according to the right hand rule, and the starting place of the knotter is shown in Fig. 13(a). And the knotting process is accordance with the time sequence of the 8 movements. L_{61} rotates around L_6 to form the tracks of the Movement I. S_{I}, S_{II}, S_{VII}, and S_{VIII} are formed when generatrices L_{11}, L_{51}, L_{41}, L_{42} rotates around pivots L_1, L_5, L_4 and L_4, respectively. The locking plane S_{I} on the knotter driving pulley is used for the standstill position of the circular rotating components which are the actuators of movements II-VI. Depends on the parameters decided above, the rotating shafts and lines in different movements are constructed uniquely as follows:

$$\boldsymbol{L}_1, \ \begin{pmatrix}x\\ y\\ z\end{pmatrix} = \begin{pmatrix}0\\ 0\\ \boldsymbol{R}\end{pmatrix}, \quad (22)$$

$$\boldsymbol{L}_2, \ \begin{pmatrix}x\\ y\\ z\end{pmatrix} = \begin{pmatrix}13.2\\ -79.0\\ 8.9\end{pmatrix} + k\begin{pmatrix}1.9\\ -80.7\\ 11.4\end{pmatrix}, k \in \mathbf{R}, \quad (23)$$

$$\boldsymbol{L}_3, \ \begin{pmatrix}x\\ y\\ z\end{pmatrix} = \begin{pmatrix}-26.8\\ -52.8\\ 2\end{pmatrix} + k\begin{pmatrix}-36.9\\ -78.0\\ 13.8\end{pmatrix}, k \in \mathbf{R}, \quad (24)$$

$$\boldsymbol{L}_4, \ \begin{pmatrix}x\\ y\\ z\end{pmatrix} = \begin{pmatrix}-38.7\\ -44.1\\ 47.5\end{pmatrix} + k\begin{pmatrix}36.8\\ -15.7\\ -8.1\end{pmatrix}, k \in \mathbf{R}, \quad (25)$$

$$\boldsymbol{L}_5,\ \begin{pmatrix}x\\y\\z\end{pmatrix}=\begin{pmatrix}-29.1\\-164.1\\50.4\end{pmatrix}+k\begin{pmatrix}65.2\\-9.3\\0\end{pmatrix},\ k\in\mathbf{R}, \tag{26}$$

$$\boldsymbol{L}_{61},\ \begin{cases}x-21.6=\rho\cos\theta,\\ y-541.3=\rho\sin\theta,\\ z-50.4=0,\end{cases}\ \theta\in[-\pi/4,\ \pi/4], \tag{27}$$

where ρ is length of the oscillating bar of the needle mechanism, 574 mm. In the *XYZ* spatial system, the tracks for holding the twine L_{51}(movement II), cutting the twine L_{41}(movement VII) and stripping off the twine L_{42} (movement VIII) are shown as Eqs. (27)–(29). And the outline of L_{42} is consistent with the outline of *CC*' part of the ϕ type knot and the configuration of the knot hook.

$$\boldsymbol{L}_{41},\ \begin{pmatrix}x\\y\\z\end{pmatrix}=\begin{pmatrix}-40.2\\-165.4\\6.8\end{pmatrix}+k\begin{pmatrix}7.3\\32.3\\-14.1\end{pmatrix},\ k\in[0,\ \ 1], \tag{28}$$

$$\boldsymbol{L}_{42},\begin{pmatrix}x\\y\\z\end{pmatrix}=\begin{pmatrix}1.2t_{C42}^2-0.2t_{C42}^3-6.2t_{C42}+71.8\\0.6t_{C42}^3-2.7t_{C42}^2+2t_{C42}-143.3\\0.4t_{C42}^2-0.1t_{C42}^3-0.7t_{C42}+23.6\end{pmatrix},\ t_{42}\in[1,8], \tag{29}$$

$$\boldsymbol{L}_{51},\ \begin{pmatrix}x\\y\\z\end{pmatrix}=\begin{pmatrix}-29.1\\-164.1\\50.4\end{pmatrix}+k\begin{pmatrix}65.2\\-9.3\\0\end{pmatrix},\ k\in[0,\ 1], \tag{30}$$

where $\boldsymbol{L}_i$ (i=1,⋯, 5) are the vector quantities of the axis L_i. $\boldsymbol{L}_{ij}$ (i=1,⋯, 5; j=1,⋯, 5) are the vector quantities of the tracks. Then the spatial tracks of S_{I}, S_{II}, S_{VII}, and S_{VIII} are as follows:

$$\boldsymbol{S}_{\mathrm{I}},\ \begin{cases}|\boldsymbol{C}_{11}\boldsymbol{C}_1|=|\boldsymbol{C}'_{11}\boldsymbol{C}_1|,\\ \cos\theta=\dfrac{\boldsymbol{C}'_{11}\boldsymbol{C}_1\cdot\boldsymbol{C}'_{11}\boldsymbol{C}_1}{|\boldsymbol{C}_{11}\boldsymbol{C}_1|\cdot|\boldsymbol{C}'_{11}\boldsymbol{C}_1|},\\ \boldsymbol{C}_{11}\boldsymbol{C}_1\cdot\boldsymbol{L}_1=0,\end{cases}\ \theta\in[0,\ 2\pi], \tag{31}$$

$$\boldsymbol{S}_{\mathrm{II}},\ \begin{cases}|\boldsymbol{C}_{51}\boldsymbol{C}_5|=|\boldsymbol{C}'_{51}\boldsymbol{C}_5|,\\ \cos\theta=\dfrac{\boldsymbol{C}_{51}\boldsymbol{C}_5\cdot\boldsymbol{C}'_{51}\boldsymbol{C}_5}{|\boldsymbol{C}_{51}\boldsymbol{C}_5|\cdot|\boldsymbol{C}'_{51}\boldsymbol{C}_5|},\\ \boldsymbol{C}_{51}\boldsymbol{C}_5\cdot\boldsymbol{L}_5=0,\end{cases}\ \theta\in[0,\ \pi/4], \tag{32}$$

$$\boldsymbol{S}_{\mathrm{VII}},\ \begin{cases}|\boldsymbol{C}_{41}\boldsymbol{C}_4|=|\boldsymbol{C}'_{41}\boldsymbol{C}_4|,\\ \cos\theta=\dfrac{\boldsymbol{C}_{41}\boldsymbol{C}_4\cdot\boldsymbol{C}'_{41}\boldsymbol{C}_4}{|\boldsymbol{C}_{41}\boldsymbol{C}_4|\cdot|\boldsymbol{C}'_{41}\boldsymbol{C}_4|},\\ \boldsymbol{C}_{41}\boldsymbol{C}_4\cdot\boldsymbol{L}_4=0,\end{cases}\ \theta\in[0,\ 26°], \tag{33}$$

$$\boldsymbol{S}_{\mathrm{VIII}},\ \begin{cases}|\boldsymbol{C}_{42}\boldsymbol{C}'_4|=|\boldsymbol{C}'_{42}\boldsymbol{C}'_4|,\\ \cos\theta=\dfrac{\boldsymbol{C}_{42}\boldsymbol{C}'\cdot\boldsymbol{C}'_{42}\boldsymbol{C}'_4}{|\boldsymbol{C}_{42}\boldsymbol{C}'_4|\cdot|\boldsymbol{C}'_{42}\boldsymbol{C}'_4|},\\ \boldsymbol{C}_{42}\boldsymbol{C}'_4\cdot\boldsymbol{L}_4=0,\end{cases}\ \theta\in[0,\ 26°], \tag{34}$$

where C_{11}, C_{51}, C_{41}, C_{42}, are the arbitrary points on the lines L_{11}, L_{51}, L_{41}, L_{42}, respectively, while points C_1, C_5, C_4, C'_4 are the foot points of them and locate on the lines L_1, L_5, L_4, L'_4, respectively. Their vector quantities are $\boldsymbol{C}_{11}$, $\boldsymbol{C}_{51}$, $\boldsymbol{C}_{41}$, $\boldsymbol{C}_{42}$, $\boldsymbol{C}_1$, $\boldsymbol{C}_5$, $\boldsymbol{C}_4$, $\boldsymbol{C}'_4$. Then the ϕ type knot is formed

$$CC',\ \ |\boldsymbol{C}_{43}-\boldsymbol{C}_3|=a(1+\cos\theta),\ \theta\in[0,\ 2\pi],$$

$$CA,\ \begin{pmatrix}x\\y\\z\end{pmatrix}=-\begin{pmatrix}0.7\\0.2\\1.1\end{pmatrix}t^3+\begin{pmatrix}3.6\\3.5\\7.5\end{pmatrix}t^2-\begin{pmatrix}14.1\\13.4\\17.1\end{pmatrix}t+\begin{pmatrix}75.7\\-143.6\\-6.0\end{pmatrix},\ t\in[0,\ 1], \tag{35}$$

where C_3—Point on the L_3,

C—Interaction point of CC' and CA curves,

A—Interaction point of CA curve and surface S_{II}.

Finally, the ϕ-type-knots knotter is figured out.

4 Experiment

4.1 Facilities and methods

The knotter was tested on the knotter test bench (Fig. 14) and in the field of Henan province located in Hwang-Huai-Hai plain (Fig. 15).

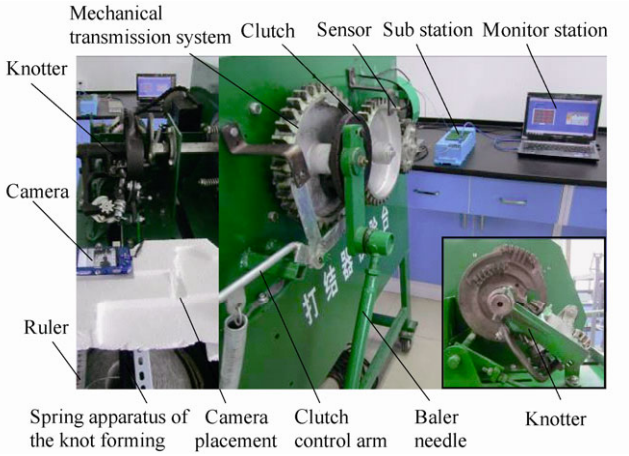

Fig. 14. Knotter test bench

(a) In field covered with wheat straws

(b) In field covered with maize straws

Fig. 15. Field experiments of ϕ-type-knots knotter

The knotter test bench consists of hardware and software systems. The hardware system includes the mechanical transmission system, the clutch, the clutch control arm, the baler needle, etc. In the operation process, the knotter is running once the clutch engaged. The power is transmitted from the mechanical transmission system to the knotter. Meanwhile, the software system consists of theupper computer, i.e., a PC monitor (use ADVANTECH WEBACCESS 7.0 software) and the sub station, i.e., an ADAM 5 510KW programmable logic controller(use MULTIPROG 4.0 software). The knotting velocity and theoretical total formed knot number could be monitored in this system by using speed sensors (SZMB-9/T-03). The change of knotting force is also measured by spring apparatus and records by the video while maximum force during the knotting process is analyzed manually.

After the wheat harvest, the field is covered with stubbles of about 20 cm long and chopped straws of about 8 cm long. The designed knotter is equipped on the 9YKZ-1.9 type square baler (Henan Haofeng Machinery Manufacturing Co. Ltd) to make the knots. The moisture of the wheat straw covered on the field is about 18% at the experiment, and the bale density is 100–120 kg/m^3. And the experiment in the maize field is done with the standing maize straws. And the knotter is equipped on the 4FYK-170 type straw chopping and baling square balers. The moisture of the maize straw was about 65%, and the bale density was 550–600 kg/m^3.

The experiment was carried out when the ϕ-type-knots knotter worked at the velocity of 75 r/min in the laboratory and field experiment. The knotter accomplished 200 knots in lab, baled 2.3 ha (500 bales with size of 360 mm×460 mm×600 mm were formed) wheat straws and 0.5 ha (200 bales with size of 360 mm×460 mm×230 mm were formed) maize straws in field. The polypropylene rope used in the experiment was 2.5 mm.

4.2 Measured parameters

4.2.1 Knotting rate

The knotting rate is the basic requirement of the performance of the knotter[27], defined as

$$S_h = \frac{n_d - n_s}{n_d} \times 100\%, \quad (36)$$

where n_d is the theoretical formed knot, and n_s is the missed knot in the experiment.

4.2.2 Maximum force during the knotting process

The maximum force during the knotting process is relevant with the bale density[39]. Therefore, 30 knots were randomly chosen from the well-formed knots in the lab experiment to measure this parameter.

4.2.3 Twine length out of the knot

The twine length out of the ϕ type knot is the effective length from the cut end to the knot, which may be relevant to the stability of the formed knot. The 30 chosen knots in the indoor experiment were measured while 10 formed knots of the compacted wheat and maize balers were also randomly chosen to be measured.

4.2.4 Breaking force of the formed knot

To test the breaking force of the formed knots, the loops of the twines are cut in the middle, and then they are installed on the clamps of the RGM-4005 Material Testing machine (Shenzhen Reger Instrument Co. Ltd) with the knots in the middle. In the testing progress, the machine stretches the knots at the velocity of 5 mm/min and the preload of 0–10 N until the knots snapped (shown in Fig. 16).

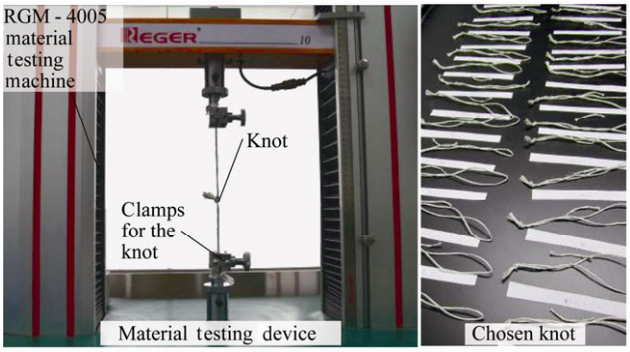

Fig. 16. Testing device for the breaking force

4.3 Statistical analysis

Mean values were calculated for the measured variables and correlation analysis was used to assess the statistical effects of maximum force during the knotting process on the twine length out of the knots and the breaking force of the formed knots. The SPSS 17.0 analytical software package was used for all of the statistical analyses.

5 Results and Discussion

As shown in Table 1, the knotting rate of the ϕ-type-knots knotter reaches 100.0% in the lab experiment, while reaches 99.6% and 100.0% in the wheat and maize field experiments, respectively. This meets the basic requirements of knotter performance in the mechanical industry standard[35]. The average maximum force at knotting process is 194.7 N. The length out of the knots formed in lab is 25.9 mm, 15.9%–20.6% lower than the knots formed in the field. Since the length out of the knots is determined by the cutting place of the knife, the differences of the length at different experimental places are caused by the different vibration.

The affordable force of the knots formed in the wheat and maize field are 115.9% and 167.2% higher, respectively, than those of the knots formed in lab due to the higher preload and interactions with the compacted bales. And the

breaking forces of the knots formed in all the experiments are larger than the existed interaction force between the twine and the compacted bales.

Table 1. Experiment results

Test type		Preload /N	Knotting rate/%	Maximum force /N	Length out of knots/mm	Breaking force of knots/N
Lab	Mean	5.3	100	194.7	25.9	212.1
	SD	0.6	–	24.1	2.4	66.1
Wheat field	Mean	31.2	99.5	–	30.8	457.9
	SD	1.3	–	–	2.6	104.7
Maize field	Mean	45.2	100	–	32.6	566.7
	SD	2.1	–	–	1.5	67.6

In the lab experiment, the breaking force of the knots formed in the lab experiment is highly ($P<0.01$) quadratic correlated with the maximum force during the knotting process (Fig. 17). When the maximum forces during the knotting processes are lower than 155.0 N, the formed loops of the knots are loose, and then the material testing machine strengthens them again when testing the breaking force by stretching them. Therefore, the breaking forces of these kinds of knots are unpredictable. When the maximum forces during the knotting processes are higher than 150.0 N, the knots are formed tighter as the maximum forces during the knotting processes are higher. Therefore, the breaking forces needed to break up the knots are higher.

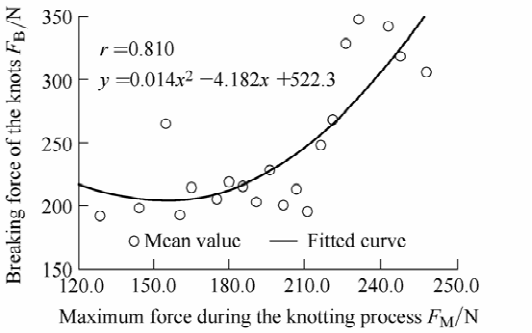

Fig. 17. Correlation between the breaking forces of the knots and the maximum forces during the knotting processes

6 Conclusions

(1) The parameters of the twines fabricated in China, the working conditions and requirements of the knotters, and the basic requirements of the knotters equipped on Chinese small rectangular balers are summarized by considering the characteristics of the compressed straws formed in Chinese small rectangular balers,

(2) The ϕ-type-knots knotter with twine holding gear mechanism, worm-helical gear mechanism, knotter hook gear mechanism, and cam mechanism is designed to realize the 8 knotting movements by using novel design paths from the mechanism structures, the time sequence and the spatial distributions aspects. According to working processes and designed parameters of the key mechanisms, the time sequences of the ϕ-type-knots knotters are figured out. The mathematical model of the knotter is also determined uniquely.

(3) In the lab experiments, the ϕ-type-knots knotter shows good performances of forming knots. Highly relevant relationship exists between the breaking force of the formed knots and the maximum force in the forming process of the knots.

(4) In the field experiments, the knotting rate of the ϕ-type-knots knotter reaches 99.6% in the wheat field and 100.0% in the maize field. The formed knots can tie up the straw bales reliably. The results prove the feasibility of the knotters.

References

[1] China's Rural Energy Yearbook. *2006 Rural energy yearbook of China*[M]. Beijing: China Agricultural Press, 2007.

[2] ZENG X Y, MA Y T, MA L R. Utilization of straw in biomass energy in China[J]. *Renewable and Sustainable Energy Reviews*, 2007, 11(5): 976–987.

[3] LIU H T, POLENSKE R K, XI Y M, et al. Comprehensive evaluation of effects of straw-based electricity generation: A Chinese case[J]. *Energy Policy*, 2010, 38(10): 6 153–6 160.

[4] WANG Y J, BI Y Y, GAO C Y. The assessment and utilization of straw resources in China[J]. *Agricultural Sciences in China*, 2010, 9(12): 1 807–1 815.

[5] GORDON M W. A transnational machine on the world stage: representing McCormick's reaper through world's fairs, 1851–1902[J]. *Journal of Historical Geography*, 2007, 33(2): 352–376.

[6] APPLEBY J F. Knotter mechanism for grain binders: US, 335 332[P]. 1886-02-02.

[7] SMITH C M. Knotter mechanism for grain binders: US, 2 815 234[P]. 1957-12-03.

[8] SCHULDT C F. Knotter: US, 3 441 302[P]. 1969-04-29.

[9] HOMBERG H E. Twine knotter for baling presses: US, 4 735 446[P]. 1988-04-05.

[10] COLLINS R H. Knotter for twine balers: US, 2 815 234[P]. 1957-12-03.

[11] SULLIVAN H D, Bledsoe B L. Knotter hook for balers: US, 3 101 963[P]. 1963-08-27.

[12] PRELLWITZ H D.. Knotting device for baling presses: EP, 0 956 761 (A1)[P]. 1999-11-17.

[13] SCHUMACHER H G. Knotter hook and cord knotter with the same: EP, 1 401 710 (A1) [P]. 2004-03-31.

[14] WERNER T. Knotting device for a big bale press: EP, 1 493 326 (A1)[P]. 2005-01-05.

[15] VINCENT R D. Knotting device: EP, 1 532 859 (A1)[P]. 2005-05-25.

[16] BALDAUF J A, ENSMINGER N K, BARNES E L. Knotter blower for agricultural balers: US, 7 318 376[P]. 2008-01-15.

[17] LIU H, JIANG G M, ZHUANG H Y, et al. Distribution, utilization structure and potential of biomass resources in rural China: With special references of crop residues[J]. *Renewable and Sustainable Energy Reviews*, 2008, 12(5): 1 402–1 418.

[18] MA J T *China's statistical yearbook*[EB/OL]. Beijing: National Bureau of Statistics of China, 2008. http://www.stats.gov.cn/.

[19] YANG S J. *Dynamic simulation and structure analysis about hay bale knotter*[D]. Beijing: Beijing Institute of Machinery Industry, 2006. (in Chinese)

[20] SU G. *Reverse engineering used on the designing of the square baler*

knotter[D]. Xinjiang: Xinjiang Agricultural University, 2006. (in Chinese)
[21] LI H, LI H W, HE J, et al. Reconstruction and optimal design of driving dentate disc of D-bale knotter based on reverse engineering[J]. *Transactions of the Chinese Society of Agricultural Engineering*, 2010, 26(5): 96–102. (in Chinese)
[22] YIN J J, LI S, LI Y M. Kinematic simulation and time series analysis of D-knotter and its ancillary mechanisms[J]. *Transactions of the Chinese Society for Agricultural Machinery*, 2011, 42(6): 103–107. (in Chinese)
[23] HUANG W, ZHANG Z Y, LIU Z Q, et al. Pro/Engineer imitation and the analysis on movements and functions of twine knott[J]. *Journal of Agricultural Mechanization Research*, 2009(9): 58–60. (in Chinese)
[24] LI H, WANG Q J, HE J, et al. Experimental research on performance of different knotter driving pulleys[J]. *Transactions of the Chinese Society of Agricultural Engineering*, 2012, 28(7): 27–33. (in Chinese)
[25] LI H, HE J, LI H W, et al. Spatial parameters of knotters of square balers[J]. *Transactions of the Chinese Society for Agricultural Machinery*, 2013, 44(8): 99–105.
[26] China's Machinery Industry Standard. JB/T9 702-2010 Knotters of rectangular balers[S]. Beijing: China Machine Press, 2010. (in Chinese)
[27] Chinese Academy of Agricultural Mechanization Sciences. *Agricultural machinery design Handbook*[M]. Beijing: China Agriculture Science and Technology Press, 2007. (in Chinese)
[28] LI X Y. *Rheodynamic characteristics of herbage materials in compression and optimization of compression process*[D]. Hohhot: Inner Mongolia Agricultural University, 2006. (in Chinese)
[29] WANG C G. *The study on rheological characteristics of hay in high density compressing*[D]. Beijing: China Agricultural University, 1998. (in Chinese)
[30] SHINNERS K J, BINVERSIE B N, MUCK R E, et al. *Comparison of wet and dry corn stover harvest and storage*[J]. *Biomass and Bioenergy*, 2007, 31(4): 211–221.
[31] ZHAO H G. *Research of the dynamic characteristics simulation of the forage baler*[D]. Harbin: Northeast Forestry University, 2007. (in Chinese)
[32] MANI S, TABIL L G, SOKHANSANJ S. Specific energy requirement for compacting corn stover[J]. *Bioresource Technology*, 2006, 97(12): 1 420–1 426.
[33] YAN Q, XIONG J J, QIU T. Safety factor with two-indexes of reliability and confidence levels[J]. *Journal of University of Science and Technology Beijing*, 2011, 33(6): 766–770. (in Chinese)
[34] DONG X Z, LI H T, WEI W J. Meshing theory and design of involute gear pair with variable shaft angle[J]. *Chinese Journal of Mechanical Engineering*, 2008, 44(7): 79–84. (in Chinese)
[35] SUN J D, FU W Y, LEI H, et al. Rotational swashplate pulse continuously variable transmission based on helical gear axial meshing transmission[J]. *Chinese Journal of Mechanical Engineering*, 2012, 25(6): 1 138–1 143.
[36] CHENG D X. *Standard handbook of mechanical design* [M]. 4th ed. Beijing: Chemical Industry Press, 2010. (in Chinese)
[37] The People's Republic of China General Administration of Quality Supervision, Inspection and Quarantine of China National Standardization Management Committee. GB/T 1357-2008 *Cylindrical gears for general engineering and for heavy engineering– Modules*[S]. Beijing: China Standards Press, 2009. (in Chinese)
[38] SUN N. *The research on digital design platform of the kontter*[D]. China Agricultural University, 2011. (in Chinese)
[39] Sperry New Holland. 05 007 711 Super 77 Twine Tie Baler[EB/OL]. USA, USA New Holland Agriculture Machinery Corporation Ltd, 2011. http: //www.dmcretail.com/newholland/.

Biographical notes

LI Hui, born in 1984, has received her PhD degree from *Beijing Key Laboratory of Optimized Design for Modern Agricultural Equipment, College of Engineering, China Agricultural University, China*, in 2013. Her research interests include square baler design and conservation tillage systems.
Tel: +86-10-62737632; E-mail: lihui657@cau.edu.cn

HE Jin, born in 1979, is currently an associated professor at *Beijing Key Laboratory of Optimized Design for Modern Agricultural Equipment, College of Engineering, China Agricultural University, China*. He received his PhD degree from *China Agricultural University* in 2007.
Tel: +86-10-62737300; E-mail: hejin@cau.edu.cn

WANG Qingjie, born in 1979, is currently a lecturer at *Beijing Key Laboratory of Optimized Design for Modern Agricultural Equipment, College of Engineering, China Agricultural University, China.* He received his PhD degree from *China Agricultural Universtiy*, in 2009.
E-mail: wangqingjie@cau.edu.cn

LI Hongwen, born in 1968, is currently a professor at *Beijing Key Laboratory of Optimized Design for Modern Agricultural Equipment, College of Engineering, China Agricultural University, China*.
E-mail: lihongwen@cau.edu.cn

RASAILY Rabi Gautam, born in 1975, has received his PhD degree from *China Agricultural Universtiy, China*, in 2012. His research interest is conservation tillage equipments and works at *Henan Hao Feng Machinery Manufacturing Co., Ltd. and Agricultural Engineering Division, Nepal Agricultural Research Council, Nepal*.

CAO Qingchun, born in 1964, is currently an engineer at *Henan Hao Feng Machinery Manufacturing Co., Ltd., China.*

ZHANG Xiangcai, born in 1987, is currently a master candidate at *Beijing Key Laboratory of Optimized Design for Modern Agricultural Equipment, College of Engineering, China Agricultural University, China*.